Single-Crystalline Co Nanowires: Synthesis, Thermal Stability, and Carbon Coating

ARTICLE *in* CHEMISTRY OF MATERIALS · AUGUST 2009

Impact Factor: 8.35 · DOI: 10.1021/cm901349y

7 AUTHORS, INCLUDING:

Frédéric Dumestre
Institut National des Sciences Appliquées de T…
19 PUBLICATIONS **941** CITATIONS
SEE PROFILE

Bruno Chaudret
French National Centre for Scientific Research
277 PUBLICATIONS **9,075** CITATIONS
SEE PROFILE

Marina Spasova
University of Duisburg-Essen
84 PUBLICATIONS **2,375** CITATIONS
SEE PROFILE

Michael Farle
University of Duisburg-Essen
257 PUBLICATIONS **5,899** CITATIONS
SEE PROFILE

Langmuir

Article

pubs.acs.org/Langmuir

Effect of a Side Reaction Involving Structural Changes of the Surfactants on the Shape Control of Cobalt Nanoparticles

Miguel Comesaña-Hermo,[†,‡,§] Robert Estivill,[†,‡] Diana Ciuculescu,[†,‡] Zi-An Li,[§] Marina Spasova,[§] Michael Farle,[§] and Catherine Amiens*[,†,‡]

[†]Laboratoire de Chimie de Coordination, CNRS, 205 route de Narbonne, F-31077 Toulouse, France

[‡]UPS, INPT; LCC, Université de Toulouse, F-31077 Toulouse, France

[§]Fakultät für Physik and Center for Nanointegration (CeNIDE), Universität Duisburg-Essen, Lotharstrasse 1, 47048 Duisburg, Germany

Supporting Information

ABSTRACT: Cobalt nanoparticles with different sizes and morphologies including spheres, rods, disks, and hexagonal prisms have been synthesized through the decomposition of the olefinic precursor $[Co(\eta^3\text{-}C_8H_{13})(\eta^4\text{-}C_8H_{12})]$ under dihydrogen, in the presence of hexadecylamine and different rhodamine derivatives, or aromatic carboxylic acids. UV−vis spectroscopy, X-ray diffraction, low and high resolution transmission electron microscopy, and electron tomography have been used to characterize the nanomaterials. Especially, the Co nanodisks formed present characteristics that make them ideal nanocrystals for applications such as magnetic data storage. Focusing on their growth process, we have evidenced that a reaction between hexadecylamine and rhodamine B occurs during the formation of these Co nanodisks. This reaction limits the amount of free acid and amine, usually at the origin of the formation of single crystal Co rods and wires, in the growth medium of the nanocrystals. As a consequence, a growth mechanism based on the structure of the preformed seeds rather than oriented attachment or template assisted growth is postulated to explain the formation of the nanodisks.

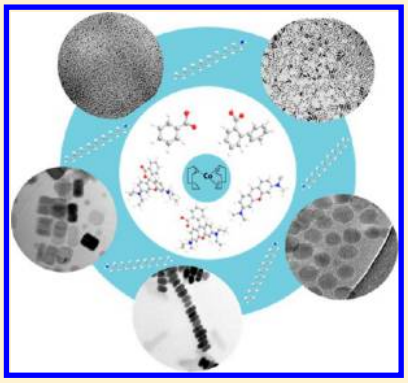

INTRODUCTION

Magnetic nanoparticles (NPs) are emerging as one of the most relevant fields of research in nanotechnology due to their broad range of applications.[1] Among them, cobalt NPs with a hexagonal closed-packed (hcp) structure are particularly interesting candidates in fields like the magnetic storage of information and the design of permanent magnets due to their high magnetization and magnetocrystalline anisotropy energy. Moreover, they present a remarkable activity as catalysts in different chemical reactions like the Fischer−Tropsch[2] and the Pauson−Khand[3] processes. These applications require a tight control over size and morphology of the objects and/or the presence of clean surfaces (absence of oxidation) and negligible effect of the adsorbed molecules on the magnetic properties of the crystals: a tight control of the synthetic parameters is thus mandatory.

The first paper dealing with the synthesis of hcp-Co NPs in which shape control was achieved was published in 1995.[4] In this study the authors presented the formation of Co single domain magnetic nanodisks with distorted hcp structure obtained from the decomposition of cobalt hydroxide in basic water solutions through reduction with hydrazine. However, the fact that they were synthesized in water leads to the uncontrolled presence of a cobalt oxide coating, which leads us to question the usefulness of this approach. During the past decades the thermal decomposition of organometallic precursors in hot surfactant solutions (mostly acids, amines, and phosphines) at relatively high temperatures has emerged as the most popular method for the synthesis of metallic Co NPs.[5−7] A representative example of this technique is the work by Puntes and co-workers,[8] who have synthesized hcp-Co nanodisks thanks to the different adsorption kinetics of oleic acid and linear amines at different crystallographic facets. Under these conditions, however, the ligands also promote Ostwald ripening of the anisotropic particles over time, leading to the formation of spherical objects as final product. With a similar procedure, Gräf and co-workers have developed the synthesis of Co nanocubes,[9] but here the structural analysis of the product obtained shows a combination of hcp-Co and ε-Co and surface oxidation. Another method for the synthesis of hcp-Co anisotropic NPs is the use of liquid polyols as both solvent and reducing agent. In these conditions, authors have obtained Co nanorods[10] and wires[11] with outstanding morphology control. Other works have used hydrothermal conditions for the production of hcp-Co nanobelts[12] and cubic nanoskeletons.[13]

Received: February 7, 2014
Revised: March 28, 2014

   dx.doi.org/10.1021/la5005165 | *Langmuir* XXXX, XXX, XXX−XXX

To date, the most advanced method for the production of fully metallic hcp-Co NPs is the reduction of the cobalt complexes $[Co(\eta^3\text{-}C_8H_{13})(\eta^4\text{-}C_8H_{12})]$ and $[Co\{N(SiMe_3)_2\}_2.thf]$ under dihydrogen using long aliphatic carboxylic acids and amines as stabilizers.[14−17] With this approach NPs with different sizes and morphologies, ranging from spherical NPs with a diameter of 3 nm to highly anisotropic objects like nanorods or nanowires with lengths above the μm, have been obtained depending on the reaction conditions. Moreover, none of these NPs present any trace of oxidation.

Recently, we have reported the formation of disk-shaped Co NPs[18] using a similar approach to that previously reported by Chaudret and co-workers. The main difference resides in the use of rhodamine B (RhB) instead of a carboxylic acid with a long aliphatic chain—variation that leads to a different growth direction. As far as we know, despite the fact that several rhodamine derivatives have been used in colloidal chemistry e.g. for the functionalization of metallic, semiconductor, or magnetic NPs aiming at the development of dye-sensitized solar cells,[19,20] or the synthesis of hybrid multifunctional magnetic−luminescent nanocomposites,[21] this family of organic dyes has never been used to tune the anisotropic growth of metallic nanocrystals. It is noteworthy that the disk-shaped Co NPs formed in the presence of RhB are the only ones reported to date displaying an easy axis of magnetization oriented perpendicular to the basis of the disk. It makes them remarkable objects for the development of high-density media for magnetic data storage which nowadays heavily relies on perpendicular recording/reading technology. They promise to be a cheap alternative to media obtained by physical processes.

Here we supplement the work presented before on the synthesis of these Co nanodisks with a study of the key parameters for their anisotropic growth. We report on the role of the various functional groups constituting the structural skeleton of RhB (carboxylic acid, amine, ammonium chloride, and aromatic rings) that could participate in the shape control of the particles via specific coordination or supramolecular organization (soft template), following a strategy based on the replacement of RhB by other molecules mimicking a part of its chemical structure. We give evidence of a side reaction between hexadecylamine and rhodamine B, the role of which is primordial in controlling the ratio of acid and amine moieties in the reacting medium. Moreover, we discuss the consequence it has on the final shape of the NPs.

EXPERIMENTAL SECTION

Materials and Methods. H_2 gas (99.995%) was purchased from Air Liquide. Rhodamine B (RhB) (95%), benzoic acid (>99.5%), biphenyl-2-carboxylic acid (98%), pyronin Y (≥45%), and rhodamine B base (97%) were purchased from Sigma-Aldrich. Hexadecylamine (HDA) (>99%) was from Fluka, and ((1,5-cyclooctadiene)(cyclooctadienyl)Co(I)) $[Co(\eta^3\text{-}C_8H_{13})(\eta^4\text{-}C_8H_{12})]$ was from Nanomeps. Rhodamine B was dried over P_2O_5 before use while the other reactants were used as received. Anisole (>99%) was purchased from Sigma-Aldrich and distilled over Na. Dried toluene and THF were obtained from a solvent purification system MBraun SPS-800. All solvents were degassed by a freeze−pump−thaw process before use.

All the synthetic protocols were carried out using standard Schlenk techniques under an Ar atmosphere to avoid contact with air or moisture. Reactions under pressure were performed in Fisher-Porter bottles, which resist pressures up to 8 bar. All glassware was kept in the oven before introduction inside the glovebox for their use. The system connecting the Fisher-Porter bottle and the H_2 bottle was purged by three successive vacuum/H_2 cycles.

Synthesis. • Seven Co nanoparticle samples (S1, S3, S4, S5, S6, S7, and S8; see Table 1) were synthesized as described hereafter: 276 mg (1 mmol) of $[Co(\eta^3\text{-}C_8H_{13})(\eta^4\text{-}C_8H_{12})]$, 1 mmol of the selected stabilizing agent (rhodamine derivative or model carboxylic acid) (see Table 1), and 241 mg (1 mmol) of HDA were introduced inside a Fisher-Porter bottle. Afterward, 20 mL of anisole was added and a suspension was formed. The bottle was pressurized with a dynamic pressure of 3 bar of H_2 for 15 min. After this period of time, it was transferred into a mineral oil bath previously thermostated at 150 °C. After 48 h the Fisher-Porter bottle was removed from the oil bath and cooled down to room temperature. At this point we observed a black solid deposited on the stirring bar (except for sample 3 (S3), see Table 1, for which a stable dark brown solution was obtained). The excess of H_2 was removed and the solvent evacuated with a canula. The black solid was washed 3 times with anisole to remove the excess of ligands, and finally the product was stored in the glovebox for further analysis. In the case of S3, the solvent was evaporated and the solid dried under vacuum.

Table 1. Samples Synthesized

derivative used (1 mmol)	amount of HDA (mmol)	sample
rhodamine B	1	S1
rhodamine B base	0	S3
rhodamine B base	0.5	S4
rhodamine B base	1	S5
pyronin Y	1	S6
benzoic acid	1	S7
biphenyl-2-carboxylic acid	1	S8

Sample 1 (S1) presents a singularity: at the end of the reaction two different solids were observed: a blue precipitate that remained in the bottom of the Fischer−Porter bottle and a black solid stuck to the stirring bar. The blue solid was isolated and stored under argon to avoid any oxidation prior to characterization. The black solid was treated as described above.

• Synthesis of Sample 2 (S2): decomposition of $[Co(\eta^3\text{-}C_8H_{13})(\eta^4\text{-}C_8H_{12})]$ in the presence of the molecular complex $[Co(Cl)_4(HDAH)_2]$. 138 mg (0.5 mmol) of $[Co(\eta^3\text{-}C_8H_{13})(\eta^4\text{-}C_8H_{12})]$ and 1 equiv of the blue $[CoCl_4(HDAH)_2]$ complex were added inside a Fischer-Porter bottle together with 20 mL of anisole. The bottle was pressurized with a dynamic pressure of 3 bar of H_2 for 15 min and H_2 then introduced in a mineral oil bath at 150 °C for 48 h. After this period of time a black precipitate was observed on the stirring bar. The excess of H_2 was evacuated and the solution removed via a canula. The black product (<10 mg) was collected with the help of a magnet and stored inside the glovebox for further analysis.

• Synthesis of worm-like nanoparticles, sample 9, was carried out as follows: Decomposition of $[Co(\eta^3\text{-}C_8H_{13})(\eta^4\text{-}C_8H_{12})]$ in the presence of HDA (S9). In a typical synthesis 276 mg (1 mmol) of $[Co(\eta^3\text{-}C_8H_{13})(\eta^4\text{-}C_8H_{12})]$ and 241 mg (1 mmol) of HDA were introduced inside a Fisher-Porter bottle. Afterward, 20 mL of toluene was added, and a brown solution was formed. The bottle was pressurized with a dynamic pressure of 3 bar of H_2 for 15 min. Subsequently, it was introduced in a mineral oil bath previously thermostated at 110 °C. After 48 h the Fisher-Porter bottle was removed from the oil bath and cooled down to room temperature. The black solid obtained was washed 3 times with toluene to remove the excess of ligands, and finally the product was stored in the glovebox for further analysis.

Characterization Techniques. *Electron Microscopy.* The nanoobjects were deposited on carbon-coated copper grids by casting a drop of a THF solution of their crude powders. TEM images were obtained on a JEOL JEM 1011 (100 kV) at the TEMSCAN facility of the University Paul Sabatier in Toulouse. Size histograms were drawn after measuring at least 100 NPs with the help of ImageJ. Results are given as "average size (standard deviation)" in nm. HREM studies were carried out on a JEOL JEM 2100F (200 kV) at the same facility and on a Philips FEI/Tecnai F20ST microscope (field emission gun, Super-Twin lens) with an operating voltage of 200 kV and a point

dx.doi.org/10.1021/la5005165 | Langmuir XXXX, XXX, XXX−XXX

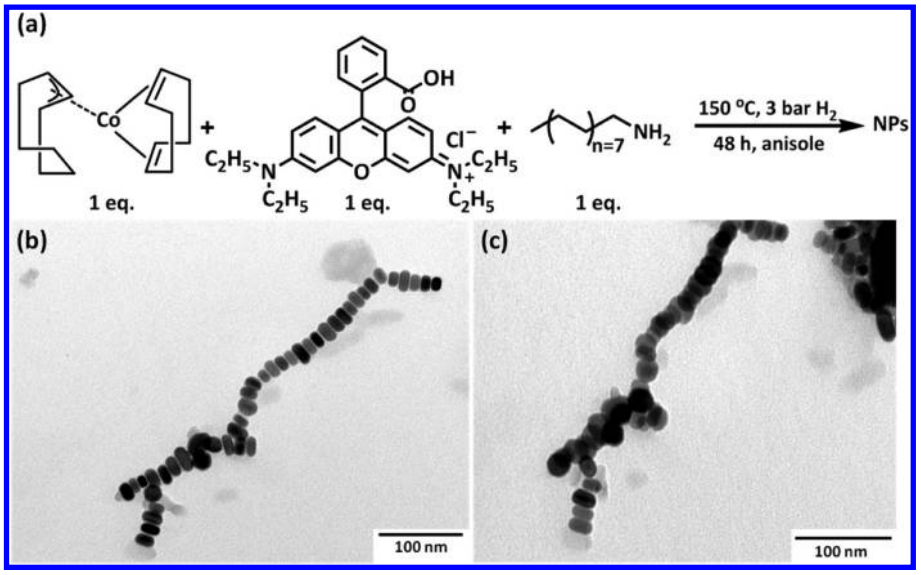

Figure 1. Reaction scheme (a) and TEM images of the nanodisks obtained in sample 1 (S1) recorded at (0°) tilting angle (b) and with a tilting angle of (45°) (c) allowing the observation of the disk-like shape of the NPs.

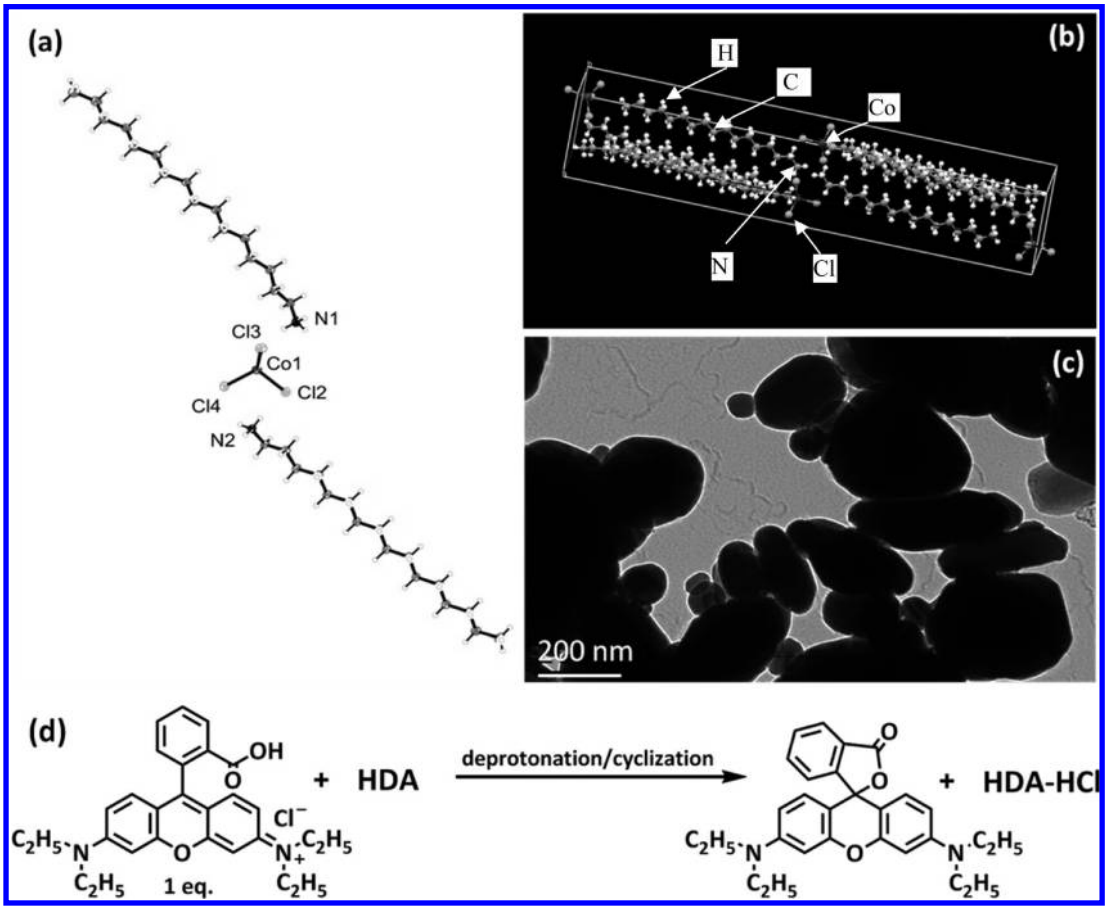

Figure 2. (a) Structure and (b) spatial arrangement of the Co^{2+} complex: H atoms in white, C ones in gray, Cl ones in light gray, and N atoms in black. (c) NPs obtained in S2. (d) Reaction scheme for the cyclization of RhB in apolar solvents.

resolution 0.24 nm, in Duisburg. Structural analysis of the images was carried out with Digital Micrograph software. The 3D structure of the Co nanoprisms was determined using electron tomography in a scanning TEM (STEM) mode, FEI's automated tilt-series acquisition software Xplore 3D, and Fischione single-tilt tomography holder on the Philips FEI/Tecnai microscope. In total, 66 electron micrographs were acquired with an acquisition time of 30 s for each micrograph and over an angle range of ±65° with tilt intervals of 2°. These micrographs were aligned and then reconstructed using the simultaneous iterative reconstruction algorithm (SIRT) implemented in the Inspect3D package. After 3D reconstruction, volumetric analysis including 3D visualization and segmentation was done using the Amira 5.0 software.

dx.doi.org/10.1021/la5005165 | *Langmuir* XXXX, XXX, XXX−XXX

X-ray Crystallography Studies. Diffraction data were collected at low temperature (180 K) on a Bruker Kappa Apex II diffractometer using a graphite-monochromated Mo Kα radiation (λ = 0.710 73 Å). The diffractometer was equipped with an Oxford Cryosystems Cryostream cooler device. The structure was solved by direct methods, and all non-hydrogen atoms were refined anisotropically using the least-squares method on F^2 with the aid of the program SHELXL-97.[22]

UV−vis Spectroscopy. Absorption spectra were recorded on a SPECORD 205 (Analytical Jena) spectrometer over the range 300−1000 nm in airtight cells with a 10 mm of optical path.

Elemental Analysis. Quantification of the metal content in S1 has been determined by ICP-MS (inductively coupled plasma−mass spectrometry). This has been done by Antellis, a company settled in Toulouse (France) that provides results validated according to ISO specifications. % Co: 97%.

RESULTS

Decomposition of the organometallic precursor $[Co(\eta^3\text{-}C_8H_{13})(\eta^4\text{-}C_8H_{12})]$ in the presence of 1 equiv of RhB and 1 equiv of HDA at 150 °C leads, after 48 h of reaction, to the formation of disk-shaped Co NPs (S1) (Figure 1) as reported in ref 18. Dispersion of the nanodisks obtained in S1 in methanol leads to a pink fluorescent solution supporting the release of RhB from the surface of the Co NPs (see Figure SI1). However, this represents only a minor fraction of the RhB introduced initially, as the organic content in the powder represents no more than 3% of the total mass (according to elemental analysis). Thus, excess RhB is certainly present in solution. The UV−vis spectrum of the solution (not shown) does not show the characteristic absorbance of RhB, suggesting that it is present only in its closed basic form, which is colorless (observation confirmed by the absence of any fluorescence from this solution). This is most probably due to the tendency of RhB to cyclize in nonpolar solvents and basic conditions (here presence of HDA) as depicted in Figure 2d.

A closer inspection of the reacting medium shows the concomitant formation of a blue precipitate. This blue solid was isolated and recrystallized in a mixture of anisole and methanol (1:1), and the crystals obtained were studied by X-ray diffraction (see Supporting Information). The diffraction data show that the actual molecule consists in a Co^{2+} center linked to four chloride anions, with Co−Cl distances ranging between 2.25 and 2.28 Å in a tetrahedral symmetry and two hexadecylammonium cations completing the structure: $[CoCl_4(HDAH)_2]$ (Figure 2a,b). The formation of this complex supposes (1) the generation of HDA-HCl in the reacting medium and (2) oxidation of Co (I) into Co(II) ions which can be puzzling at first sight when working in a reducing atmosphere of H_2. The oxidation process is confirmed by two independent observations: $[CoCl_4(HDAH)_2]$ is not reduced by H_2 even at 150 °C, and oxidation of Co(I) into Co(II) species occurs upon addition of HDA-HCl to $[Co(\eta^3\text{-}C_8H_{13})(\eta^4\text{-}C_8H_{12})]$. The formation of HDA-HCl is easily explained as a consequence of the reaction between RhB and HDA already discussed above (Figure 2d).

Recently, it was shown[23] that side reactions taking place in the complex mixtures involved in the synthesis of Co NPs may become the key parameter defining the characteristics of the nanocrystals. Here, as the $[CoCl_4(HDAH)_2]$ complex displays a lamellar arrangement, it could participate in the anisotropic growth of the NPs. Actually, if the tendency toward lamellar organization persisted in solution, the complex could act as a template in which the preformed seeds would grow, following a preferential direction.[24] To ascertain this possibility, we performed a control experiment in which $[Co(\eta^3\text{-}C_8H_{13})(\eta^4\text{-}C_8H_{12})]$ was decomposed in the presence of $[CoCl_4(HDAH)_2]$ alone, keeping the rest of the parameters constant (time, temperature, solvent, and H_2 pressure) (S2). At the end of the reaction no disk-shaped NPs could be evidenced. Actually, only polydisperse NPs with sizes above 200 nm were observed on the TEM grid (Figure 2c), excluding therefore the template-assisted mechanism as the reason for the formation of the long chains of disks. On the other hand, the $[CoCl_4(HDAH)_2]$ complex could also participate as a reservoir of Co atoms during the formation of the nanodisks. Nevertheless, this possibility was discarded due to the impossibility to decompose this complex under the conditions of reaction used to synthesize the disks.

At this stage, $[CoCl_4(HDAH)_2]$ looks like a thermodynamic dead end in the synthetic process.

We then investigated the role played by the cyclized form of the RhB issued from the side reaction (RhB base) on the anisotropic growth of the NPs. When it is used as only stabilizer, keeping the other parameters constant, large agglomerates of Co NPs with a large size distribution (ranging between 12 and 50 nm in diameter) are observed (S3) (see Figure SI2). On the other hand, when the synthesis is performed with 0.5 or 1 mmol of HDA, better control over the final morphology of the particles is achieved.

When only 0.5 mmol of HDA is added (S4), hexagonal nanoprisms are obtained as the only product as evidenced by tomography experiments (Figure 3). Interestingly, these nanoprisms present structural defects along their *c*-axis as evidenced by the appearance of the (0001) and (000−1) forbidden reflections (Figure 3f).

If 1 mmol of the HDA is added, anisotropic NPs are formed (S5) (Figure 4a). Tilting experiments have been performed to ascertain the final morphology of the objects (Figure 4b,c). We can conclude that this sample consists in hcp-Co nanorods with their *c*-axis lying along the direction of preferential growth. These nanorods present a diameter of 30.7 (5) nm and an aspect ratio of 2.46. Interestingly, they also display stacking faults along their *c*-axis (Figure 4d,e).[18]

The particles obtained in S4 and S5 present an important similarity with the nanodisks synthesized with RhB (S1): in all three cases we observe stacking faults along the *c*-axis. Interestingly, an increase in the concentration of HDA in solution leads to the growth of the {10−10} facets at the expense of the {0001} ones.

To better understand the system, we tried to ascertain the role played by the different functional groups present in RhB and RhB base (the fused aromatic rings with tendency to π-stacking, the ammonium chloride side group, etc.). Thus, we carried out control experiments in which RhB was substituted by other molecules that represent part of its structure (Figure 5), together with control experiments with aromatic carboxylic acids and pure HDA.

In the first place, pyronin Y (PY) has been chosen to determine the influence of the aromatic rings together with the tertiary amine and the ammonium chloride present in the structure. When PY and HDA are used as stabilizers, 8 (0.9) nm Co NPs and a population of micrometer size irregular objects (S6) are obtained (Figure 6a). Even though the majority of the NPs are single crystalline spherical NPs with hexagonal morphology, a small population of them presents structural defects in the form of twin planes. Once again, tilting

dx.doi.org/10.1021/la5005165 | *Langmuir* XXXX, XXX, XXX−XXX

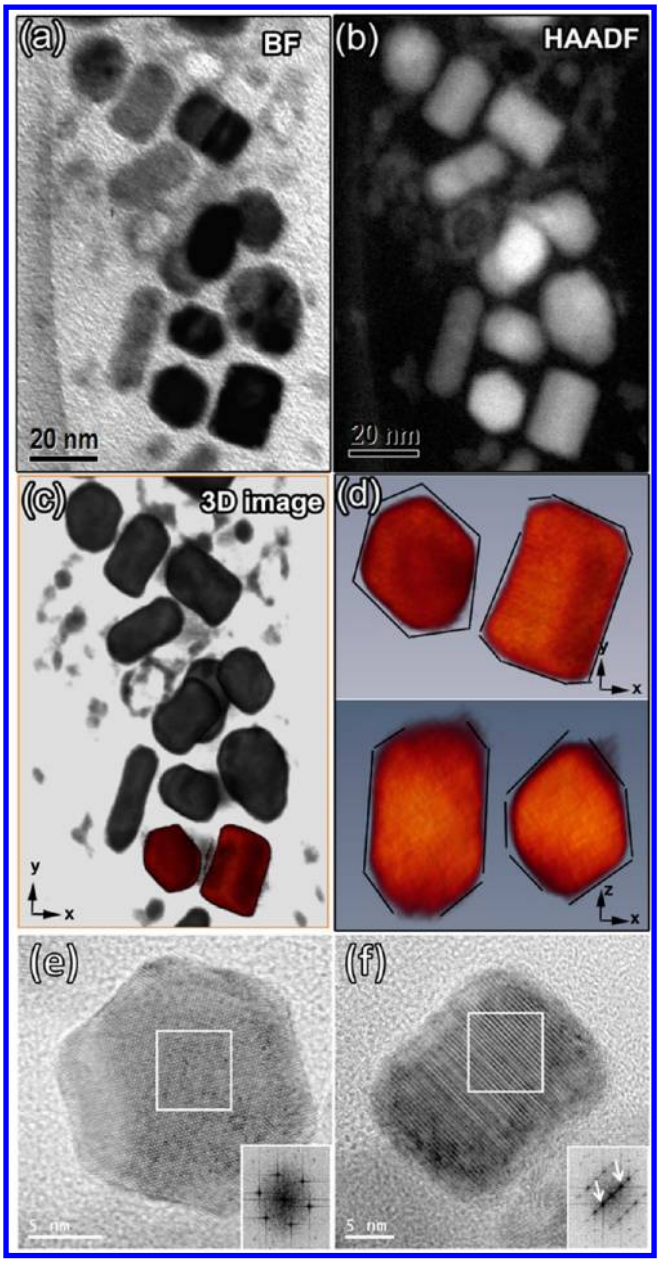

Figure 3. (a–d) TEM images of an ensemble of Co nanoprisms. (a) Bright-field (BF) TEM image, (b) high-angle annular dark field (HAADF) image, and (c) 3D volume-rendered image. (d) The two nanoprisms situated in the lower part of image (c) were oriented along different directions so that the prism-like morphologies and the well-defined hexagonal facets can be seen clearly. (e, f) HREM images of two nanoprisms with their *c*-axis lying perpendicular (e) and parallel (f) to the grid. The insets in the images are the FFTs of the corresponding white squares. The white arrows in the inset of image f indicate the presence of the forbidden reflections associated with the presence of structural defects.

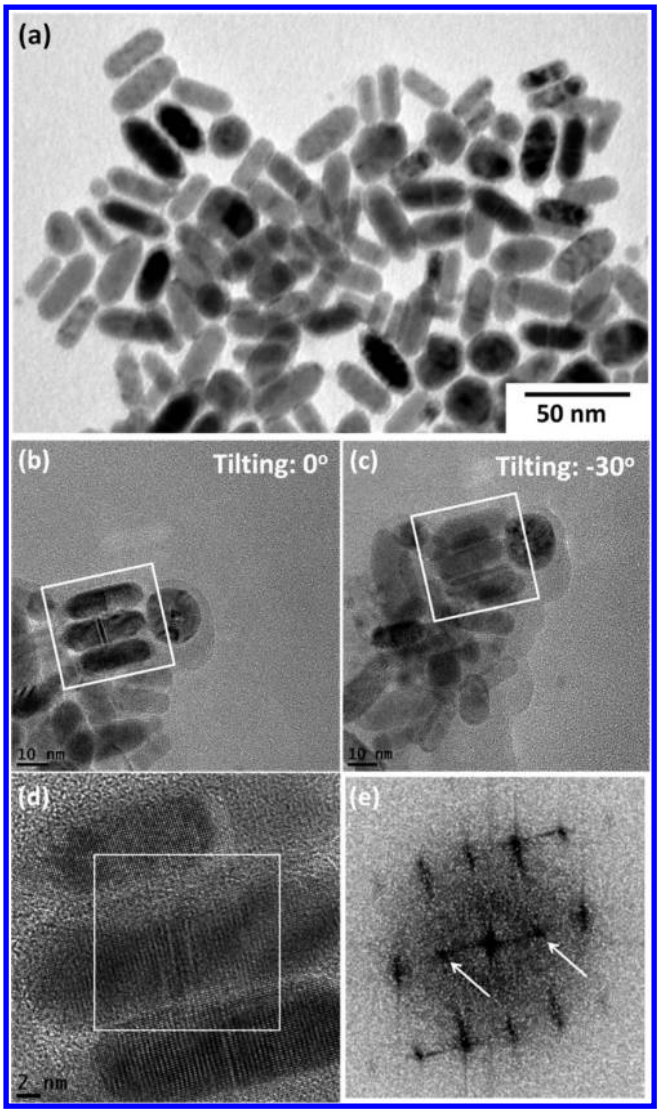

Figure 4. (a–c) TEM images showing the rod-shaped NPs formed in sample S5. (d, e) HREM image and structural analysis by FFT of the nanorods. The white arrows in (e) indicate the presence of the (0001) and (000−1) forbidden reflections.

experiments have been performed in order to elucidate the actual morphology of the objects, recording images at different degrees of tilt (Figure 6b,c). This study showed that only the NPs with stacking faults present an anisotropic morphology (Figure 6d). In comparison with the nanodisks obtained in S1 here the anisotropic particles present smaller size and aspect ratio (1.41) between length and thickness. The difference in the final shape of the particles obtained here seems to be related with the morphology of the original seed: single crystalline seeds lead to the formation of a spherical particle while the 2D growth should be favored over the isotropic one if the seeds present twin planes.[25,26]

Next, we used benzoic acid and biphenyl-2-carboxylic acid as model molecules to understand the effect of the aromatic carboxylic acid moiety present in the chemical structure of the RhB. These acids are expected to interact more weakly with the Co surface than long chain carboxylic acids due to their conjugation with the aromatic ring. Their packing density at the surface of the nanoparticles could also be different.[27] The TEM images of the sample obtained in the presence of benzoic acid (S7) show the formation of small spherical NPs with a mean diameter of 2.2 (0.5) nm (Figure 7).

When biphenyl-2-carboxylic acid is used as substituent of RhB in the reaction, we observe the formation of two kinds of NPs: spherical NPs with a diameter of 5.5 (0.6) nm and nanorods with the same diameter and an aspect ratio of 3.45 (S8, Figure 8). The larger volume of the spherical particles obtained here (as compared to S7) could be a direct consequence of the higher steric hindrance of the acid used.

dx.doi.org/10.1021/la5005165 | *Langmuir* XXXX, XXX, XXX−XXX

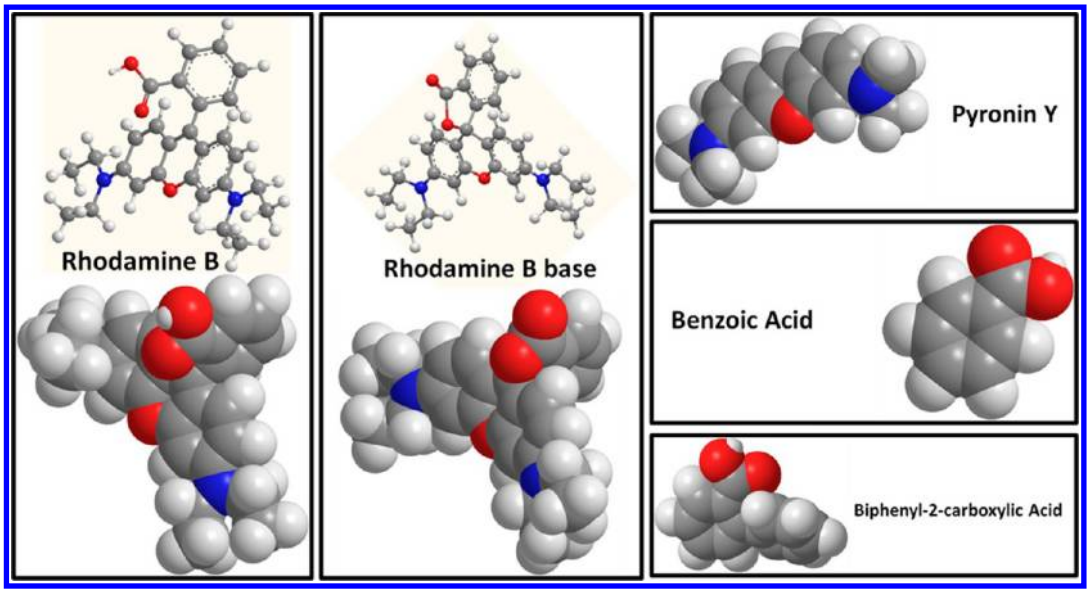

Figure 5. 3D rendering of the ligands used in this study (O in red, N in blue, C in gray, and H in white color, obtained from ChemBio 3D Ultra 13.0 (the structures have been obtained after performing MM2 energy minimization calculations).

Tilting experiments show that the anisotropic NPs are actually nanorods rather than nanodisks,[28] excluding therefore any similarity between the growth mechanism of S1 and S8 (see Figure SI3). Moreover, analysis of HREM images shows that they are single crystals without any structural defect (Figure 5b), but displaying slightly corrugated faces. It is noteworthy that the diameter of the rods perfectly matches that of the isolated NPs, in agreement with an anisotropic growth via an oriented attachment process.

Last, the role of HDA was investigated. Amines with long aliphatic chains have been of general use during the past years as ligands in the synthesis of anisotropic NPs, either alone[29] or together with other surfactants.[30] Our previous studies show that these molecules play a crucial role in the synthesis of anisotropic Co particles like nanorods and nanowires, most probably because they facilitate the formation of carboxylate complexes and/or the formation of supramolecular assemblies.[16] In the present study, decomposition of the organometallic precursor under the same conditions but in the absence of this amine results in the formation of Co objects without any morphological control, evidencing the mandatory presence of HDA (see Figure SI4). Actually, when HDA is used as the only stabilizer during the decomposition of the Co precursor (S9), anisotropic objects are obtained (Figure 9). These NPs present an almost one-directional growth following the *c* direction. Nevertheless, and in opposition to similar objects obtained when aliphatic carboxylic acids are present in the reaction medium, stacking faults and irregular surfaces appear. It is noteworthy that the formation of similar worm-like nano-objects containing staking faults has been reported in the case of Pt NPs when HDA was used as the sole stabilizing ligand.[31]

DISCUSSION

All the work presented above has been carried out with a simple goal: trying to unravel the reasons behind the formation of the unusual hcp-Co nanodisks, given the huge interest for the development of high density media for magnetic data storage or rare-earth-free permanent magnets.[18]

Three models are usually discussed to explain the formation of the anisotropic Co nano-objects: (1) the anisotropic growth is governed by the crystallographic structure of the seed formed in the early stages of the reaction;[25,26] (2) anisotropic superstructures forming during the reaction process like micelles, vesicles, or supramolecular complexes with long-range order can direct the preferential growth of the crystals following a template-assisted mechanism;[32−34] (3) specific adsorption of surfactants at crystallographic facets can facilitate their growth at the expense of other facets, thus directing the anisotropic growth of the particle.[35] At first sight, each of these three models or a combination of them could account for the formation of the Co nanodisks, given the complexity of the medium.

Formation of the $[Co(Cl)_4(HDAH)_2]$ complex in the reaction medium clearly evidences the occurrence of a side reaction leading to the cyclization of RhB, thus blocking the carboxylic acid function. Furthermore, this study points out that disk shaped NPs can only be obtained when using RhB base or PY as ligands (samples 1, 3, and 5), i.e., in the absence of the coordinating carboxylic acid function. It is noteworthy that aliphatic carboxylic acids under H_2 pressure are supposed to favor reconstruction of NPs leading to defect-free nanocrystals with exceptionally smooth surfaces.[14] A similar phenomenon is clearly observed here in sample 8 where single crystalline cobalt rods are obtained in the presence of biphenyl-2-carboxylic acid. However, as the Co/acid interaction and packing density are weaker for aromatic acids than for aliphatic ones,[27] the surface of the single crystalline rods still displays some corrugation, a fingerprint of the initial rounded NPs from which they originate. In contrast, in the case of sample 9, the lability of the amine[36] induces the coalescence of the intermediate nanoparticles into polycrystalline nano-objects displaying staking faults. Moreover, persistence of these defects is favored as a consequence of the weak amine/Co interaction (case of sample 9) which is apparently insufficient to induce reconstruction of the cobalt surfaces in the synthetic conditions used here.

We thus believe that in the present case the reaction between RhB and HDA helps maintaining a low quantity of carboxylic

dx.doi.org/10.1021/la5005165 | *Langmuir* XXXX, XXX, XXX−XXX

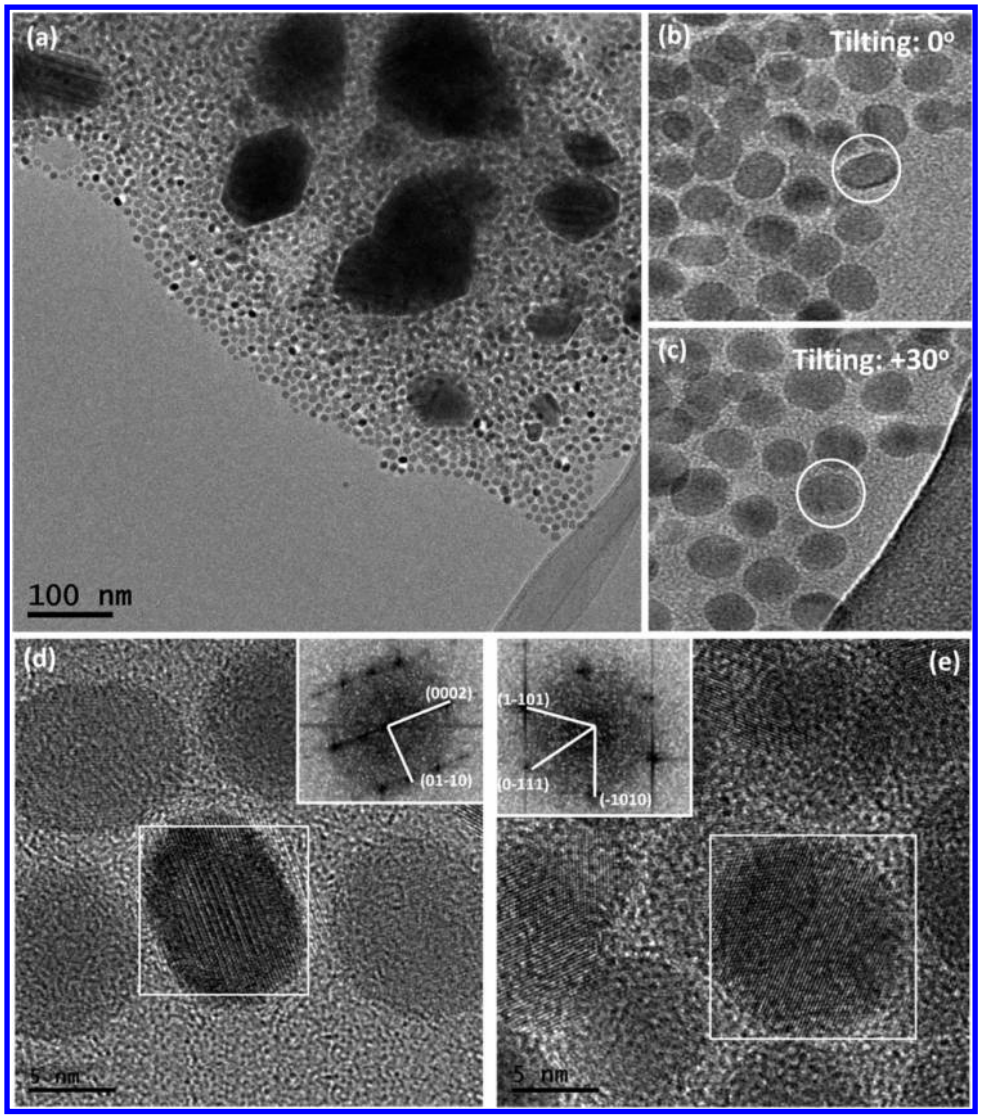

Figure 6. (a–c) TEM images of the particles obtained in S6. The white circles in (b) and (c) represent the same NP with different degrees of tilting. (d, e) HREM images of the two different NPs obtained: anisotropic with stacking faults and spherical single crystalline.

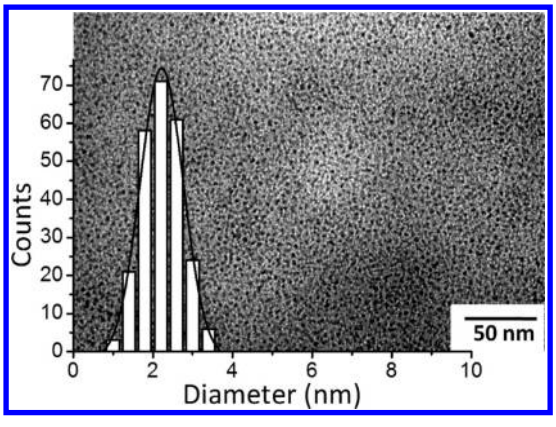

Figure 7. TEM images of the NPs obtained with benzoic acid (S7).

acid in the reacting medium. This would be detrimental to the reconstruction process even since the very beginning of the growth of the NPs, but on the other hand, it would favor the persistence of defects throughout the growth process.

A similar effect of *in situ* changes of the composition of the reaction medium on the structure and shape of nanocrystals has been recently evidenced in the case of Co multipods: when a significant quantity of carboxylic acid was present in the solution, the growth of monocrystalline multipods was favored, while polycrystalline objects were formed when the concentration of acid was low.[23]

Another interesting fact is that in the reactions S4 and S5, where a subsequent quantity of HDA molecules are available to interact with the Co surface, the growth of the more energetic {10−10} facets is favored, following the assumption that HDA has specific affinity for them, as already postulated by Puntes et al.[6] The growth of the {10−10} facets at the expense of the {0001} thus depends strongly on the amount of free amine available. This points out once again that the side reaction between RhB and HDA plays an important role on the final control over the shape of the NPs, since it is responsible for the removal of HDA from the reaction medium.

The observations presented above tend to exclude any template effect as well as specific coordination of ligands as the origin of the formation of the Co disks. They rather suggest that the presence of defects in the seed NPs due to the fast

dx.doi.org/10.1021/la5005165 | *Langmuir* XXXX, XXX, XXX−XXX

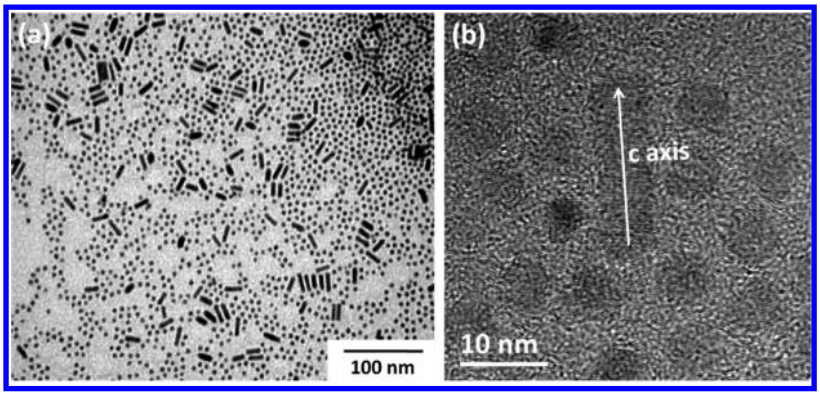

Figure 8. Low (a) and high (b) resolution TEM images of sample S8.

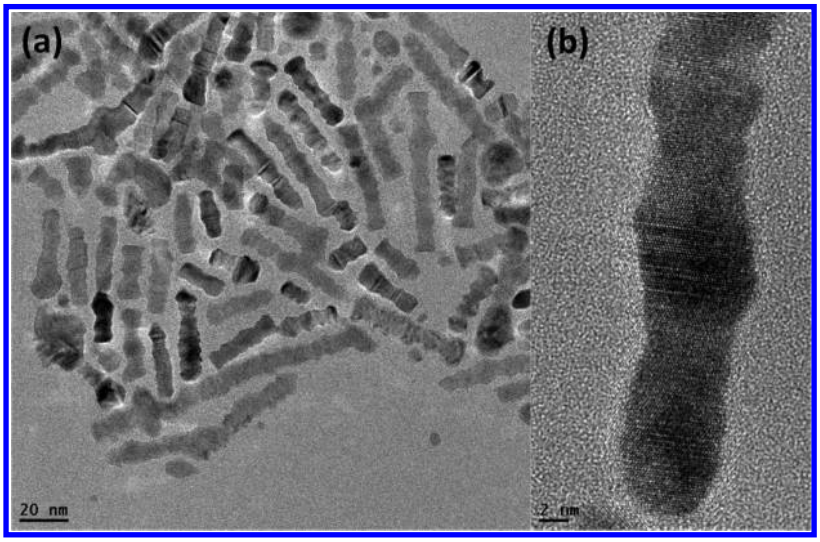

Figure 9. Low (a) and high resolution (b) TEM images of S9.

decomposition of the cobalt precursor corresponding to a burst-like nucleation step is the origin of the anisotropic growth. In this case, the presence of these defects, associated with the absence of any reconstruction/recrystallization process, as a result of the consumption of the carboxylic acid ligand by the side reaction, would induce the development of the seeds into disk-like nanoparticles, as postulated in refs 25 and 26, for the formation of silver platelets. The formation of the Co disks is thus under kinetic control rather than governed by thermodynamics.

CONCLUSION

We have presented a study of the key parameters leading to the formation of hcp-Co nanodisks in the presence of HDA and RhB ligands, NPs that can be of great interest for many applications in the near future. Calculations to evaluate the relative energy of coordination of the ligand on the corners, edges, and surfaces of the Co-disks will be carried out to ascertain their location, as this would be very useful in view of future application of these NPs in catalytic processes. In this paper, we have shown that *in situ* formation of RhB base by reaction between HDA and RhB is a key point to control the anisotropic growth of the NPs. Indeed, it helps regulate the available amount of amine and carboxylic acid in the reacting medium, promoting the development of faulted seeds. This work demonstrates that new mixtures of ligands (rhodamine derivatives in the presence of amines) can be effectively used to direct the growth of hcp-Co NPs in a controlled manner. Moreover, it once again stresses the importance of studying the occurrence of side reactions, here leading to structural and functional modifications of the ligands, to better understand the growth of nanocrystals.

ASSOCIATED CONTENT

Supporting Information

Visible spectrum of the Co nanodisks synthesized in S1 when introduced in methanol, TEM image of S3, TEM images at different tilting angles of S8, TEM image of the NPs obtained when the cobalt precursor is decomposed in the presence of RhB without HDA, and crystallographic data for $[CoCl_4(HDAH)_2$. This material is available free of charge via the Internet at http://pubs.acs.org.

AUTHOR INFORMATION

Corresponding Author

*E-mail catherine.amiens@lcc-toulouse.fr (C.A.).

Notes

The authors declare no competing financial interest.

ACKNOWLEDGMENTS

We thank Laure Vendier for X-ray analysis of sample 2. Miguel Comesaña-Hermo thanks the EC (MEST-CT-2005-020195 "Nanotool" program) for a grant and the Deutsche

Forschungsgemeinschaft and the Stiftung Mercator for financial support.

REFERENCES

(1) Lu, A.-H; Salabas, E. L.; Schuth, F. Magnetic Nanoparticles: Synthesis, Protection, Functionalization, and Application. *Angew. Chem., Int. Ed.* **2007**, *46*, 1222−1244.

(2) Khodakov, A. Y.; Chu, W.; Fongarland, P. Advances in the Development of Novel Cobalt Fischer−Tropsch Catalysts for Synthesis of Long-Chain Hydrocarbons and Clean Fuels. *Chem. Rev.* **2007**, *107*, 1692−1744.

(3) Kim, S.-W.; Son, S. U.; Lee, S. S.; Hyeon, T.; Chung, Y. K. Colloidal Cobalt Nanoparticles: a Highly Active and Reusable Pauson−Khand Catalyst. *Chem. Commun.* **2001**, *21*, 2212−2213.

(4) Gibson, C. P.; Putzer, K. J. Synthesis and Characterization of Anisometric Cobalt Nanoclusters. *Science* **1995**, *267*, 1338−1340.

(5) Dinega, D. P.; Bawendi, M. G. A Solution-Phase Chemical Approach to a New Crystal Structure of Cobalt. *Angew. Chem., Int. Ed.* **1999**, *38*, 1788−1791.

(6) Puntes, V. F.; Krishnan, K. M.; Alivisatos, P. Synthesis, Self-Assembly, and Magnetic Behavior of a Two-Dimensional Superlattice of Single-Crystal ε-Co Nanoparticles. *Appl. Phys. Lett.* **2001**, *78*, 2187−2189.

(7) Timonen, J. V. I; Seppälä, E. T.; Ikkala, O.; Ras, R. H. A. From Hot-Injection Synthesis to Heating-Up Synthesis of Cobalt Nanoparticles: Observation of Kinetically Controllable Nucleation. *Angew. Chem., Int. Ed.* **2011**, *50*, 2080−2084.

(8) Puntes, V. F.; Zanchet, D.; Erdonmez, C. K.; Alivisatos, A. P. Synthesis of hcp-Co Nanodisks. *J. Am. Chem. Soc.* **2002**, *124*, 12874−12880.

(9) Gräf, C. P.; Birringer, R.; Michels, A. Synthesis and Magnetic Properties of Cobalt Nanocubes. *Phys. Rev. B* **2006**, *73*, 212401−212405.

(10) Soumare, Y.; Garcia, C.; Maurer, T.; Chaboussant, G.; Ott, F.; Fiévet, F.; Piquemal, J.-Y.; Viau, G. Kinetically Controlled Synthesis of Hexagonally Close-Packed Cobalt Nanorods with High Magnetic Coercivity. *Adv. Funct. Mater.* **2009**, *19*, 1971−1977.

(11) Liu, Q.; Guo, X.; Chen, J.; Li, J.; Song, W.; Shen, W. Cobalt Nanowires Prepared by Heterogeneous Nucleation in Propanediol and Their Catalytic Properties. *Nanotechnology* **2008**, *19*, 365608.

(12) Xie, Q.; Dai, Z.; Huang, W.; Liang, J.; Jiang, C.; Qian, Y. Synthesis of Ferromagnetic Single-Crystalline Cobalt Nanobelts via a Surfactant-Assisted Hydrothermal Reduction Process. *Nanotechnology* **2005**, *16*, 2958.

(13) Wang, X.; Fu, H.; Peng, A.; Zhai, T.; Ma, Y.; Yuan, F.; Yao, J. One-Pot Solution Synthesis of Cubic Cobalt Nanoskeletons. *Adv. Mater.* **2009**, *21*, 1636−1640.

(14) Dumestre, F.; Chaudret, B.; Amiens, C.; Fromen, M.-C.; Casanove, M.-J.; Renaud, P.; Zurcher, P. Shape Control of Thermodynamically Stable Cobalt Nanorods through Organometallic Chemistry. *Angew. Chem., Int. Ed.* **2002**, *41*, 4286−4289.

(15) Dumestre, F.; Chaudret, B.; Amiens, C.; Respaud, M.; Fejes, P.; Renaud, P.; Zurcher, P. Unprecedented Crystalline Super-Lattices of Monodisperse Cobalt Nanorods. *Angew. Chem., Int. Ed.* **2003**, *42*, 5213−5216.

(16) Ciuculescu, D.; Dumestre, F.; Comesaña-Hermo, M.; Chaudret, B.; Spasova, M.; Farle, M.; Amiens, C. Single-Crystalline Co Nanowires: Synthesis, Thermal Stability, and Carbon Coating. *Chem. Mater.* **2009**, *21*, 3987−3995.

(17) Wetz, F.; Soulantica, K.; Respaud, M.; Falqui, A.; Chaudret, B. Synthesis and Magnetic Properties of Co Nanorod Superlattices. *Mater. Sci. Eng., C* **2007**, *27*, 1162−1166.

(18) Comesaña-Hermo, M.; Ciuculescu, D.; Li, Z.-A.; Stienen, S.; Spasova, M.; Farle, M.; Amiens, C. Stable Single Domain Co Nanodisks. Synthesis, Structure and Magnetism. *J. Mater. Chem.* **2012**, *22*, 8043−8047.

(19) Funston, A. M.; Jasieniak, J. J.; Mulvaney, P. Complete Quenching of CdSe Nanocrystal Photoluminescence by Single Dye Molecules. *Adv. Mater.* **2008**, *20*, 4274−4280.

(20) Boulesbaa, A.; Issac, A.; Stockwell, D.; Huang, Z.; Huang, J.; Guo, J.; Lian, T. Ultrafast Charge Separation at CdS Quantum Dot/Rhodamine B Molecule Interface. *J. Am. Chem. Soc.* **2007**, *129*, 15132−15133.

(21) Bertorelle, F.; Wilhelm, C.; Roger, J.; Gazeau, F.; Ménager, C.; Cabuil, V. Fluorescence-Modified Superparamagnetic Nanoparticles: Intracellular Uptake and Use in Cellular Imaging. *Langmuir* **2006**, *22*, 5385−5391.

(22) Sheldrick, G. M. A Short History of SHELX. *Acta Crystallogr.* **2008**, *A64*, 112.

(23) Liakakos, N.; Cormary, B.; Li, X.; Lecante, P.; Respaud, M.; Maron, L.; Falqui, A.; Genovese, A.; Vendier, L.; Koïnis, S.; Chaudret, B.; Soulantica, K. The Big Impact of a Small Detail: Cobalt Nanocrystal Polymorphism as a Result of Precursor Addition Rate during Stock Solution Preparation. *J. Am. Chem. Soc.* **2012**, *134*, 17922−17931.

(24) Huo, Z.; Tsung, C.-K.; Huang, W.; Zhang, X.; Yang, P. Sub-Two Nanometer Single Crystal Au Nanowires. *Nano Lett.* **2008**, *8*, 2041−2044.

(25) Lofton, C.; Sigmund, W. Mechanisms Controlling Crystal Habits of Gold and Silver Colloids. *Adv. Funct. Mater.* **2005**, *15*, 1197−1208.

(26) Xia, Y.; Xiong, Y.; Lim, B.; Skrabalak, S. E. Shape-Controlled Synthesis of Metal Nanocrystals: Simple Chemistry Meets Complex Physics? *Angew. Chem., Int. Ed.* **2009**, *48*, 60−103.

(27) Pensa, E.; Rubert, A. A.; Benitez, G.; Carro, P.; Gonzalez Orive, A.; Hernandez Creus, A.; Salvarezza, R. C.; Vericat, C. Are 4-Mercaptobenzoic Acid Self Assembled Monolayers on Au(111) a Suitable System to Test Adatom Models? *J. Phys. Chem. C* **2012**, *116*, 25765−25771.

(28) It also confirms that the spherical nanoparticles are not disks lying flat on the surface

(29) Cordente, N.; Respaud, M.; Senocq, E.; Casanove, M.-J.; Amiens, C.; Chaudret, B. Synthesis and Magnetic Properties of Nickel Nanorods. *Nano Lett.* **2001**, *1*, 565−568.

(30) Lacroix, L.-M.; Lachaize, S.; Falqui, A.; Respaud, M.; Chaudret, B. Iron Nanoparticle Growth in Organic Superstructures. *J. Am. Chem. Soc.* **2009**, *131*, 549−557.

(31) Ramirez, E.; Eradès, L.; Philippot, K.; Lecante, P.; Chaudret, B. Shape Control of Platinum Nanoparticles. *Adv. Funct. Mater.* **2007**, *17*, 2219−2228.

(32) Habas, S. E.; Lee, H.; Radmilovic, V.; Somorjai, G. A.; Yang, P. Shaping Binary Metal Nanocrystals through Epitaxial Seeded Growth. *Nat. Mater.* **2007**, *6*, 692−697.

(33) Liu, Y.; Goebl, J.; Yin, Y. Templated Synthesis of Nanostructured Materials. *Chem. Soc. Rev.* **2013**, *42*, 2610−2653.

(34) Gao, C.; Zhang, Q.; Lu, Z.; Yin, Y. Templated Synthesis of Metal Nanorods in Silica Nanotubes. *J. Am. Chem. Soc.* **2011**, *133*, 19706−19709.

(35) Kim, F.; Connor, S.; Song, H.; Kuykendall, T.; Yang, P. Platonic Gold Nanocrystals. *Angew. Chem., Int. Ed.* **2004**, *43*, 3673−3677.

(36) Pan, C.; Pelzer, K.; Philippot, K.; Chaudret, B.; Dassenoy, F.; Lecante, P.; Casanove, M.-J. Ligand-Stabilized Ruthenium Nanoparticles: Synthesis, Organization, and Dynamics. *J. Am. Chem. Soc.* **2001**, *123*, 7584−7593.